Structural basis for oligomerization and glycosaminoglycan binding of CCL5 and CCL3

Wenguang G. Liang[a], Catherine G. Triandafillou[b], Teng-Yi Huang[c], Medel Manuel L. Zulueta[c], Shiladitya Banerjee[d], Aaron R. Dinner[d,e], Shang-Cheng Hung[c,1], and Wei-Jen Tang[a,1]

[a]Ben May Department for Cancer Research, The University of Chicago, Chicago, IL 60637; [b]Graduate Program in Biophysical Sciences, The University of Chicago, Chicago, IL 60637; [c]Genomics Research Center, Academia Sinica, Taipei 115, Taiwan; [d]James Franck Institute, The University of Chicago, Chicago, IL 60637; and [e]Department of Chemistry, The University of Chicago, Chicago, IL 60637

Edited by Elias J. Lolis, Yale University, New Haven, CT, and accepted by the Editorial Board March 22, 2016 (received for review December 4, 2015)

CC chemokine ligand 5 (CCL5) and CCL3 are critical for immune surveillance and inflammation. Consequently, they are linked to the pathogenesis of many inflammatory conditions and are therapeutic targets. Oligomerization and glycosaminoglycan (GAG) binding of CCL5 and CCL3 are vital for the functions of these chemokines. Our structural and biophysical analyses of human CCL5 reveal that CCL5 oligomerization is a polymerization process in which CCL5 forms rod-shaped, double-helical oligomers. This CCL5 structure explains mutational data and offers a unified mechanism for CCL3, CCL4, and CCL5 assembly into high-molecular-weight, polydisperse oligomers. A conserved, positively charged BBXB motif is key for the binding of CC chemokines to GAG. However, this motif is partially buried when CCL3, CCL4, and CCL5 are oligomerized; thus, the mechanism by which GAG binds these chemokine oligomers has been elusive. Our structures of GAG-bound CCL5 and CCL3 oligomers reveal that these chemokine oligomers have distinct GAG-binding mechanisms. The CCL5 oligomer uses another positively charged and fully exposed motif, KKWVR, in GAG binding. However, residues from two partially buried BBXB motifs along with other residues combine to form a GAG-binding groove in the CCL3 oligomer. The N termini of CC chemokines are shown to be involved in receptor binding and oligomerization. We also report an alternative CCL3 oligomer structure that reveals how conformational changes in CCL3 N termini profoundly alter its surface properties and dimer–dimer interactions to affect GAG binding and oligomerization. Such complexity in oligomerization and GAG binding enables intricate, physiologically relevant regulation of CC chemokine functions.

signal transduction | CC chemokine | protein oligomerization | glycosaminoglycan | X-ray crystallography

The CC chemokines are a 28-member family of 8- to 14-kDa small-molecular-weight (MW) chemotactic cytokines with crucial roles in inflammation and infection (1, 2). Chemokine oligomerization and their interaction with glycosaminoglycans (GAGs), polysaccharides that are either free or attached to proteoglycans mostly on cell surface or in the extracellular matrix, is a coupled process that play key roles in chemokine functions (3–8). These include, but are not limited to, protection from proteolysis, regulation of chemotactic/haptatactic gradients to guide cell migration, transcytosis of chemokines across cells, and presentation to surface receptors of target cells, particularly under flow conditions. Most CC chemokines readily dimerize by themselves and form higher-MW complexes in the presence of GAGs (4). CC chemokine ligand 3 (CCL3) (MIP-1α), CCL4 (MIP-1β), and CCL5 (RANTES) are CCR5 ligands that are involved in diverse proinflammatory responses and are targeted for therapeutic innovations for human diseases including cancer, cardiovascular diseases, and HIV infection (9–12). Unlike other CC chemokines, these chemokines reversibly self-assemble into high-MW oligomers, up to >600 kDa in size (13, 14). The presence of GAGs further modulates the oligomerization of these chemokines. Mutants of these chemokines with reduced oligomerization have chemotactic activity comparable to wild-type chemokines (15, 16). However, such mutants make CCL3, CCL4, and CCL5 less effective at recruiting cells into the mouse peritoneum (14, 17, 18). CCL5 mutants defective in oligomerization fail to block HIV infection and induce the expression of IFN-γ and CCL4 (15, 19). Normally, CCL5 can trigger CCR5-dependent apoptosis and G protein-coupled receptor–independent MAP kinase activation via CD44, but CCL5 mutants defective in either oligomerization or GAG binding fail to elicit these responses (20, 21). Manipulation of CCL3 oligomerization by mutation has led to the development of CCL3-based cancer therapies that preserve stem cells and boost immune therapy (11, 12, 22).

Accumulating evidence indicates that oligomerization of CC chemokines occurs in vivo. For example, CCL5 is released from T cells as high-MW, GAG-bound complexes (23) and filamentous CCL5 oligomers are found on vascular endothelial cells in a GAG-dependent manner (24). However, significant gaps exist in our understanding of the structural basis of CC chemokine oligomerization and GAG binding. Although CCL3, CCL4, and CCL5 oligomerize readily under physiological conditions, only CCL3 and CCL4 oligomer structures are available at a neutral pH (14) (Table S1). All available CCL5 structures were determined at acidic pH (25–30) (Table S1). Unfortunately, none

Significance

Oligomerization and glycosaminoglycan (GAG) binding are key regulatory steps for many extracellular ligands. Our analyses provide a structural basis of CC chemokine ligand 5 (CCL5) and CCL3 oligomerization and explain how oligomerization affects the interaction of these chemokines with GAG and their functions. Our GAG-bound chemokine structures reveal how CCL5 and CCL3 oligomerization creates distinctive GAG-binding grooves to enhance GAG binding via avidity for regulating chemokine functions. Furthermore, our CCL5 structure may explain how CXCL4, a CXC chemokine, heterooligomerizes with CCL5 to modulate chemokine-mediated activities. Together, these data provide new structural insights into how oligomerization and GAG binding are coupled to regulate functions of CC chemokines and offer novel pharmacophores for the design of therapeutics for treating chemokine-mediated human diseases.

Author contributions: W.G.L. and W.-J.T. designed research; W.G.L. and W.-J.T. performed research; T.-Y.H. and S.-C.H. contributed new reagents/analytic tools; W.G.L., C.G.T., S.B., A.R.D., and W.-J.T. analyzed data; and W.G.L., C.G.T., M.M.L.Z., A.R.D., and W.-J.T. wrote the paper.

The authors declare no conflict of interest.

This article is a PNAS Direct Submission. E.J.L. is a guest editor invited by the Editorial Board.

Data deposition: The crystallography, atomic coordinates, and structure factors have been deposited in the Protein Data Bank, www.pdb.org (PDB ID codes 5COY, 5CMD, 5DNF, 5D65, and 5COR).

[1]To whom correspondence may be addressed. Email: schung@gate.sinica.edu.tw or wtang@uchicago.edu.

This article contains supporting information online at www.pnas.org/lookup/suppl/doi:10.1073/pnas.1523981113/-/DCSupplemental.

explains how CCL5 mutations profoundly affect CCL5 oligomerization and alter its biological functions (15, 16, 18–21, 31). Thus, the structural basis for CCL5 oligomerization is unknown.

Significant efforts have been made to elucidate the structural basis of GAG binding to target proteins (3, 32, 33). Such efforts reveal the structural diversity of GAGs, their target proteins, and the interaction interfaces between them. Mutational and structural studies have confirmed a role of the BBXB motif (basic/basic/x/basic residue) in CC chemokines in GAG binding, oligomerization, and receptor binding (4, 5, 14, 28, 34). Structures of CCL3 and CCL4 oligomers, however, show that the BBXB motif is located at the interface between dimers of these chemokines (14). Thus, oligomerization prevents the BBXB motif from binding GAG in the manner shown in the CCL5–GAG disaccharide structure (28). Thus, how GAG binds CC chemokine oligomers and how chemokine oligomerization affects GAG binding remain unknown. Here, we combined crystallographic, small-angle X-ray scattering (SAXS), and mathematical modeling analyses to unveil the structural basis for CCL5 oligomerization at a physiological pH. We also solved the structures of CCL3 and CCL5 oligomers in complex with synthetic heparin to elucidate the molecular basis for the interaction of CC chemokine oligomers with GAG.

Results

Structural Basis of CCL5 Oligomerization. To address the structural basis for CCL5 oligomerization, we sought to identify a crystallization condition for CCL5 at neutral pH (Table S2). We found that the naturally occurring CCL5(4-68) variant of CCL5, in which three CCL5 N-terminal residues are deleted, displays dramatically reduced CCL5 precipitation without affecting formation of high-MW oligomers. Although CCL5(4-68) could be crystalized at an acidic pH, it also formed crystals at a pH of 7.0–8.0 that was temperature-sensitive (optimal at 30 °C). Heparins, a well-known class of GAGs, have disaccharide repeats of glucosamine-iduronic acid or glucosamine-glucuronic acid that have 48 possible combinations (33). Twenty-three of 48 possible repeats have been found in vivo. To determine a GAG-bound CCL5 oligomer structure, we used synthetic heparins that have one to four N,O6-disulfoglucosamine (SGN) and O2-sulfoiduronic acid (IDS) repeats (Fig. S1*A*) (33, 35, 36). The use of synthetic heparin eliminated the complexity and chemical heterogeneity of commercially available GAGs and allowed the formation of better-diffracting crystals that had interpretable GAG density. We first solved the dimeric CCL5(4-68) structure crystallized at an acidic pH at 1.4-Å resolution then used it as a search model for molecular replacement. In conjunction with sulfur phasing, we solved the structure of CCL5(4-68) oligomer crystallized at a neutral pH in the presence and absence of heparin **8f**, a synthetic heparin octasaccharide (Fig. S1*A*) at 2.55-Å and 3.05-Å resolution, respectively (Table S2). The week-long dehydration of CCL5(4-68) crystals in the presence of **8f** significantly improved diffraction quality.

The electron density of CCL5 is generally excellent except for the 4–10 N-terminal loop (Fig. S1*B*). The structure of heparin-free CCL5(4-68) is a hexamer in an asymmetric unit (Fig. 1*A* and Movie S1), whereas that of heparin **8f**-bound CCL5(4-68) has nine monomers arranged as one and a half hexamers (Fig. S1*C*). These hexameric structures are nearly identical (Fig. S1*D*). The CCL5 hexamer can be viewed as a complex of three CCL5 dimers. Within the hexamer, the CCL5 monomer has an expected structure: an N-terminal segment (amino acids 4–20) followed by a 3_{10} helical turn (amino acids 21–23), an antiparallel three-stranded β-sheet (amino acids 24–55), and an α-helix (amino acids 55–68). The arrangement of CCL5 dimers is similar to dimeric CCL5 structures crystallized at low pH (Fig. S1 *E* and *F*) (25–30). However, the contacts between CCL5 dimers in our CCL5 oligomeric structure nicely explain how mutations affect CCL5 oligomerization and function. Between CCL5 dimers, E26 forms a salt bridge with R47 whereas E66 forms hydrogen bonds with T43 and R44 as

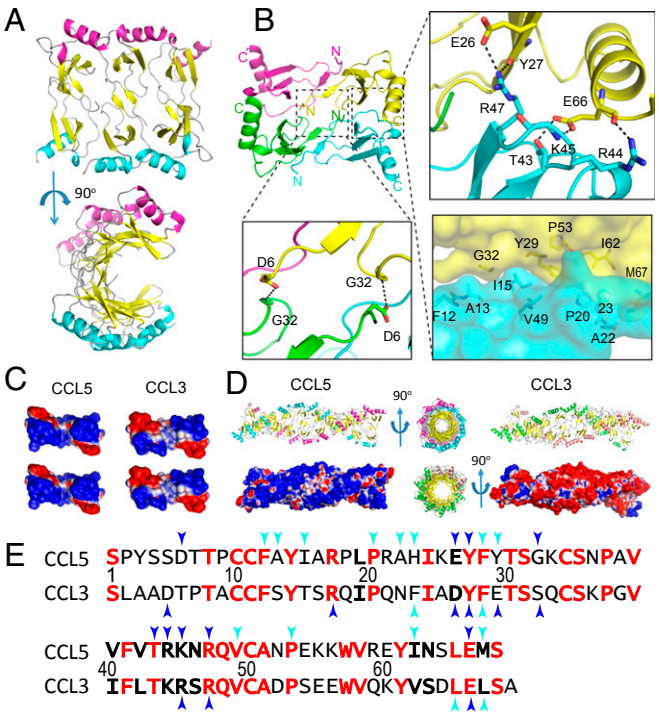

Fig. 1. Structure of CCL5(4-68) oligomer. (*A*) Ribbon representation of CCL5(4-68) hexamer (PDB ID code 5CMD). (*B*) Detailed interactions between CCL5 dimers. (*C*) Charge complementarity between CCL5 dimers and CCL3 dimers. The dimer interface is colored from negative surface (red, −1 kT) to positive (blue, +1 kT). (*D*) Comparison of CCL5 and CCL3 20mer. The PDB ID code of CCL3 oligomer is 2X69. Electrostatic surface is colored as calculated by APBS (<−1 kT in red and >+1 kT in blue). The 20mer models of CCL5 and CCL3 are built by the offset alignment and the use of symmetry-related structure, respectively. (*E*) Sequence alignment of CCL5 and CCL3. Identical and conserved residues are in red and boldface, respectively. Blue and cyan arrows indicate residues that form hydrophilic and hydrophobic interactions between CCL dimers, respectively.

well as a salt bridge with K45 (Fig. 1*B*). This explains how the mutation of E66 or E26 to serine or alanine profoundly reduces CCL5 oligomerization and decreases its functionality and mutations at the ^{44}RKNR^{47} BBXB motif also affect CCL5 oligomerization (Fig. S1*G*) (15, 16, 18–21). This structure also explains how the A22K mutation enhances CCL5 oligomerization, because this lysine would form a hydrogen bond to N63 of the adjacent CCL5 monomer (Fig. S1*H*) (31). This structure can explain how an H23K mutation reduces CCL5 oligomerization by disrupting van der Waals contacts between H23 and N63 of the two CCL5 monomers (31).

The Mechanism for Forming Double-Helical CCL5 Oligomers Is Similar to That of CCL3 and CCL4 Oligomers. The structure of CCL5(4-68) hexamer suggests that, like CCL3 and CCL4, charge and surface complementarity allow CCL5 dimers to come together and polymerize into rod-shaped double-helical oligomers that are polydisperse in size (Fig. 1 *C* and *D*) (14). Residues that form hydrophilic interactions at the dimer–dimer interfaces are highly conserved between CCL3, CCL4, and CCL5, but not other CC chemokines (Fig. 1*E* and Fig. S1 *I* and *J*). This can explain why only these chemokines self-assemble into high-MW oligomers. To probe whether wild-type CCL5 forms rod-shaped oligomers in solution, we performed SAXS analysis of CCL5 (0.5–1 mg/mL) in buffer containing Tris·HCl (pH 8) and 500 mM NaCl to prevent CCL5 from precipitating (Fig. 2*A*). If CCL5 oligomers were rod-shaped, the linearity over a range of scattering vectors in the plot of cross-section, Guinier rod would be expected. Indeed, the observed plot revealed linearity at q values ranging from 0.03 to 0.09 (Fig. 2*A*, *Inset*).

BIOCHEMISTRY

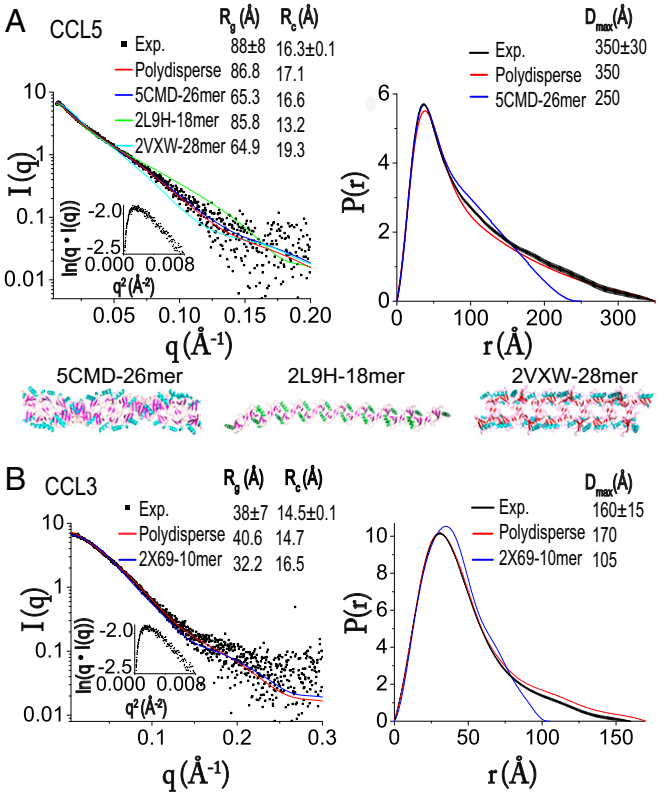

Fig. 2. SAXS scattering curve with cross-section, Guinier rod plot in inset (*Left*) and the pair distribution (*Right*) of CCL5 (*A*) and CCL3 (*B*). CCL5 data are fit with the fixed-length oligomers of three CCL5 structure models, 5CMD-26mer (26mer of CCL5 structure with PDB ID code 5CMD), 2L9H-14mer, and 2VXW-28mer shown as ribbon representation at the bottom of *A*. The length is chosen based on the optimal fitting χ values of 1.16, 1.91, and 2.03 for CCL5 5CMD-26mer, 2L9H-14mer, and 2VXW-28mer, respectively, where χ was calculated by $\chi^2 = (1/(N-1)) \times \Sigma_j((\mu I(s_j) - I_{exp}(s_j))/\sigma(s_j))^2$ (N is the number of experimental points and μ is the scaling factor). Data are also fit with the mathematical model for the formation of double-helical oligomers that are polydisperse in size (Polydisperse) using the equation for the concentration of oligomers of *k* monomers, $c(k) = \frac{c_t}{2}(1-\alpha^2)\alpha^{\left(\frac{k}{2}-1\right)}$, where α, the only fitting parameter, is directly related to the dissociation constant between dimers and c_t is the total protein concentration. The same process is used to analyze CCL3 SAXS data with either CCL3 10mer structure (PDB ID code 2X69) (2X69-10mer) or a simple polymerization model of CCL3 oligomers that are polydiperse in size (Polydiperse).

There are three available CCL5 oligomeric structures: a double-helical rod based on our CCL5(4-68) structure (PDB ID code 5CMD), a CCL5 structure derived from a hybrid method using NMR, SAXS and molecular simulation (PDB ID code 2L9H), and P2-RANTES, which has enhanced the ability of CCL5 to inhibit HIV-1 infection due to its mutated N-terminal sequences (PDB ID code 2VXW) (27, 29). All of them are rod-shaped. We first generated a oligomer model from each of the three structures that had χ values near 1 (Fig. 2*A*). We then evaluated which model best fit the experimental cross-section R_g value (R_c). We found that only the double-helical CCL5 26mer derived from our CCL5(4-68) model fit the experimental scattering curves and R_c value well (Fig. 2*A*). Although the CCL5 26mer offered the best fit among the three models, the predicted R_g and maximal dimension (D_{max}) of the CCL5 26mer (250 Å) deviated significantly from the observed D_{max} value of CCL5 (350 Å, Fig. 2*A*). We rationalize that CCL5 follows a simple polymerization mechanism, and thus should exist as an equilibrium mixture of monomers, dimers, and oligomers of different lengths (14, 37). Indeed, this model generated a pair distribution profile that fit well with the observed P(r) distribution (Fig. 2*A*). Together with existing mutational studies (15, 16, 18–21), we conclude that our double-helical CCL5 oligomer model represents how CCL5 forms polydisperse oligomers in solution under physiological conditions (Fig. S1*G*). This could also represent CCL5 filaments found on the surface of endothelial cells that are polydisperse in size (24).

Under the same experimental conditions, we found that CCL3 had a much smaller R_g (38 Å) than wild-type CCL5 (88 Å) (Fig. 2*B*). We speculate that the additional hydrophobic contacts in CCL5 could render CCL5 more prone to form high-MW oligomers than CCL3 (Fig. 1*E*). The R_g value of CCL3 was also much smaller than that of CCL3 observed in PBS (pH 7.2), which had an R_g value of 130 Å (14). This is likely because we used the higher NaCl concentration and slightly alkaline pH that could reduce the overall size of CCL3 oligomers. However, CCL3 retained its rod-shaped, polydisperse oligomeric structure (Fig. 2*B*). We also performed a SAXS analysis of CCL5(4-68) under the same condition. However, the SAXS profile of CCL5(4-68) revealed significant aggregation, which precludes meaningful interpretation (Fig. S2*B*).

Structure of Heparin 8f-Bound CCL5 and CCL3 Oligomers. To address how GAG binds CCL5 oligomers, we solved a heparin **8f**-bound CCL5 hexamer structure. Anomalous signals confirmed the position of sulfate atoms in heparin **8f** (Fig. S3 *A* and *B*). For each CCL5(4-68) hexamer, two heparin **8f** chains that contained three sugar moieties were clearly visible (Fig. 3*A* and Movie S1). The trisaccharide of **8f** binds a positively charged groove involving R17, K55, K56, and R59 of the CCL5(4-68) oligomer (Fig. 3*B*). In addition to hydrogen bonds and van der Waals contacts, K55, K56, and R59 form a network of salt bridges with the sulfate groups of SGN-I, IDS-II, and SGN-III (Fig. 3 *C* and *D*). Thus, heparin primarily binds the ^{55}KKWVR^{59} motif of the CCL5 oligomer. This is consistent with the role of positively charged residue in the ^{55}KKWVR^{59} motif for GAG binding and biological functions (e.g., the adhesion of T lymphocytes and monocytes as well as leukocyte recruitment into the mouse peritoneal cavity) (38). Previous analyses reveal that the ^{44}RKNR^{47} BBXB motif is known to be crucial for GAG binding and a structure to elucidate how heparin disaccharide binds this motif has been determined (18, 28, 34, 39). This BBXB motif, however, is largely buried in our CCL5 oligomer structure, which prevents it from binding heparin (Fig. 3*E* and Fig. S3*C*). Thus, our structure indicates that the ^{55}KKWVR^{59} motif serves as the primary site to bind GAG when CCL5 is oligomerized. Our GAG-bound CCL5 structure suggested that the presence of heparin should significantly increase the propensity of CCL5 and CCL5(4-68) to form high-MW aggregates. We probed the effect of heparin on CCL5 oligomerization by SAXS and found this to be the case (Fig. S2).

We have also solved a heparin **8f**-bound CCL3 structure at 3.1-Å resolution (Table S2 and Fig. S4). The structure contains five CCL3 monomers arranged similarly to the heparin-free CCL3 oligomer (14) and four sugar moieties in the **8f**-bound CCL3 structure (Fig. 4*A* and Fig. S4 and Movie S1). The CCL3 oligomers form a positively charged groove to bind heparin (Fig. 4*B*). Taking advantage of the fact that the ^{45}KRSR^{48} BBXB motif is only partially buried, K45 and R46 from two different BBXB motifs of CCL3 monomers form salt bridges and van der Waals contacts with SGN-I in heparin **8f** (Fig. 4*C*). In addition, Q19, N23, and K61 form salt bridges and hydrogen bonds with SGN-III and IDS-IV (Fig. 4 *C* and *D*). Furthermore, L66, D65, and Q22 form hydrophobic interactions with heparin **8f**. Interestingly, most residues involved in the binding of heparin to CCL3 and CCL5 oligomers are not well-conserved despite the high conservation of residues involved in oligomerization (Figs. 4*E* and 1*E*).

Alternative CCL3 Oligomer Structure. While seeking conditions to crystallize heparin-bound CCL3, we found a crystallization condition that formed in the presence of **8f**. We optimized the condition

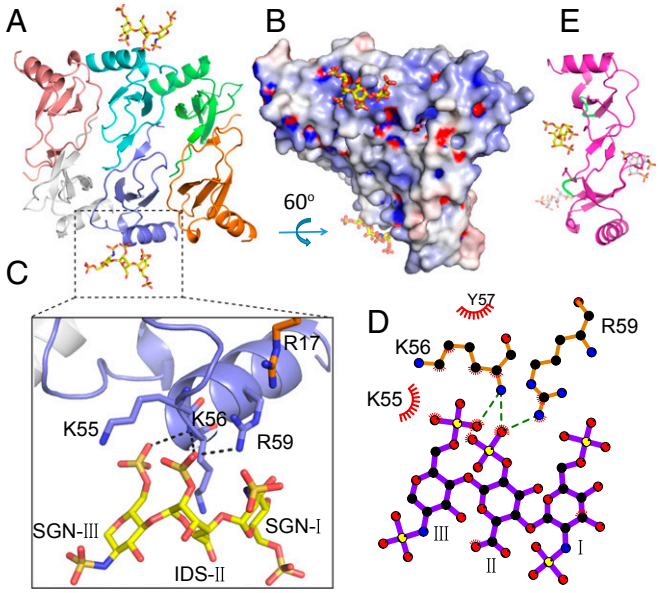

Fig. 3. Structure of heparin **8f**-bound CCL5 hexamer. (*A*) Overall structure of **8f**-bound CCL5 oligomer. CCL5 is shown in ribbon representation and colored by chain. Carbon (yellow), oxygen (red), nitrogen (blue), and sulfur (orange) of heparin are depicted in stick. (*B*) Electrostatic potential is colored from red (−10 kT) to blue (+10 kT). (*C*) Close-up view and (*D*) schematic representation of the interaction of CCL5 and heparin **8f**. Red "eyelashes" indicate hydrophobic interactions. (*E*) Ribbon representation of heparin disaccharide I-S bound CCL5 dimer (PDB ID code 1U4L).

without **8f** and solved an alternative CCL3 oligomer structure at 2.55 Å resolution (Fig. 5, Table S2, and Fig. S5*A*). This structure had 10 CCL3 molecules in an asymmetric unit, which forms a double-helical rod-shaped oligomer that is similar to the previously reported CCL3 oligomer structure (14). However, 4 out of 10 N termini pass through the interface between CCL3 dimers and point outward toward the convex part of the CCL3 oligomer instead of pointing inward to the concave cavity of the CCL3 oligomer, as previously reported (Fig. 5*A* and Movie S1) (14). Although the outward-pointing N termini do not alter the overall structures of CCL3 monomers or dimers (except the N termini) (Fig. 5*B*), they push the CCL3 dimers apart, creating a larger gap (~3 Å) between them (Fig. 5*C* and Fig. S5*B*). As a result, salt bridges and hydrogen bonds between CCL3 dimers, including those between S33–Y15, E30–R18, D27–R46, and Y28–R48, are broken (Fig. 5*C*). This leads to an overall loss of ~100 $Å^2$ of contact surface between CCL3 dimers, thus likely reducing their affinity for each other (Fig. 5*C* and Fig. S5*C*). However, the outward-pointing N termini of CCL3 form hydrogen bonds between A1–S33, S2–S33, and N34–L3, which help stabilize this structure. Interestingly, this N-terminal protrusion profoundly increases the size of the positively charged pocket on the CCL3 surface, which could bind GAG (Fig. 5*D*). This might explain why **8f** facilitates the formation of this crystal form. However, no obvious extra density existed when CCL3 was cocrystallized with **8f**. This could be due to the low occupancy constrained by a crystal lattice and/or crystallization condition.

Discussion

Based on our crystallographic, SAXS, and mathematical modeling analyses, we propose that CCL5 oligomerization follows a simple polymerization process to form rod-shaped double-helical oligomers that are polydisperse in size (Fig. 6*A*). Despite being very different in their isoelectric points and charge distribution, CCL5 has the same mechanism of oligomerization with CCL3 and CCL4 (14). Our CCL5 oligomer structure explains existing CCL5 mutational data (15, 16, 18–21, 31). Furthermore, it offers an alternative model to describe how CXCL4 enhances the arrest of CCL5-stimulated monocytes (40, 41). Instead of heterodimerization between CCL5 and CXCL4 shown by NMR under an acidic condition (40), we propose that CXCL4 can form a heterooligomer with CCL5 (Fig. S6). CXCL4 was discovered based on its high affinity to heparin, and our modeling predicts that this heterooligomer would have altered electrostatic potential that could enhance GAG binding (Fig. S6). In addition, the insertion of CXCL4 into CCL5 oligomer could also change the kinetics of CCL5 oligomerization. Together, they contribute to enhanced CCL5 function. This model is consistent with data on the effects of ^{44}RKNR^{47} and E26 mutations (41). It suggests an exciting hypothesis that chemokine function is regulated by heterooligomerization of CC and CXC chemokines that typically form distinct dimers and higher-order oligomers (5).

Our GAG-bound CC chemokine structures reveal that a novel GAG binding site can form via protein oligomerization. Structures of CC chemokine oligomers reveal the molecular basis for how a positively charged pocket in the 50s loop of CCL5 binds GAGs even though the pocket formed by the BBXB motif in the 40s loop is buried. Furthermore, they show how a novel GAG binding site can form at the interface between CCL3 dimers. These structures offer a structural explanation for how multiple GAG binding sites can form upon CCL3 and CCL5 oligomerization and strengthen the binding of these chemokines to GAG via avidity. Consistent with this notion, the binding affinities of chemokines are highly dependent on oligomerization (42).

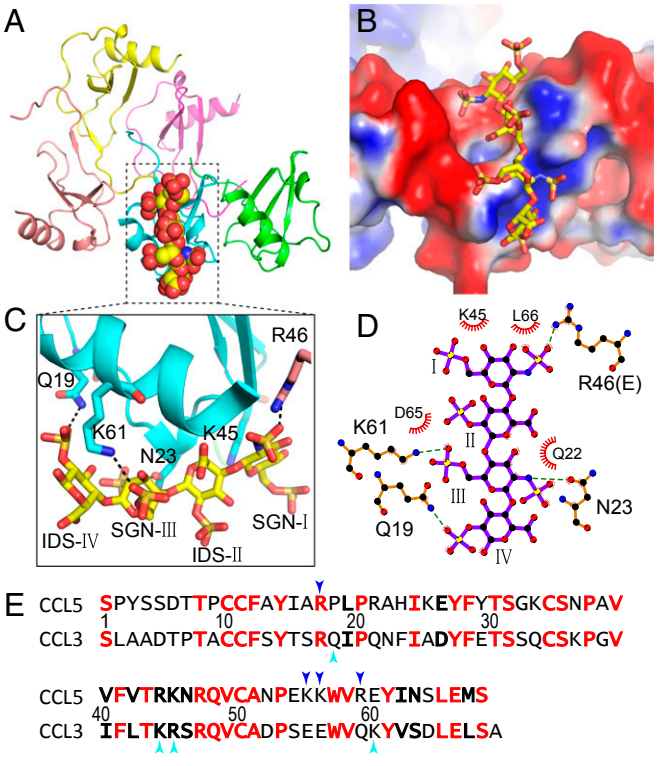

Fig. 4. Structure of heparin **8f**-bound CCL3. (*A*) Overall structure of **8f**-bound CCL3. CCL3 is shown in ribbon representation and colored by chain. Carbon (yellow), oxygen (red), nitrogen (blue), and sulfur (orange) of heparin are depicted in stick. (*B*) Electrostatic potential is colored from red (−1 kT) to blue (+1 kT). (*C*) Close-up view and (*D*) schematic representation of the interaction of CCL3 and heparin **8f**. Red "eyelashes" indicate hydrophobic interactions. (*E*) Sequence alignment of CCL5 and CCL3. Identical and conserved residues are in red and boldface, respectively. Cyan arrows indicate residues involved in the interaction of heparin with CCL3 and blue arrows indicate those with CCL5.

BIOCHEMISTRY

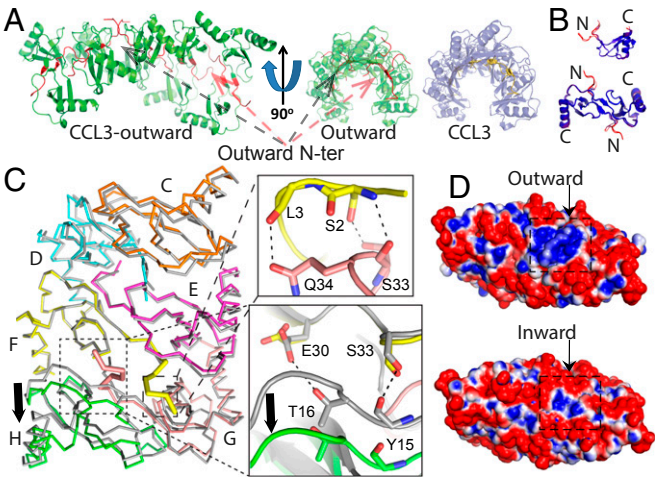

Fig. 5. Structure of alternative CCL3 oligomer. (*A*) Ribbon representation of CCL3 decamer with four N termini pointing outward and the comparison with CCL3 decamer with all N termini pointing inward. (*B*) Alignment of monomer and dimer between CCL3 pointing outward and that pointing inward. Molecule is colored by rmsd. (*C*) Alignment of CCL3 with N termini pointing outward (colored, PDB ID code 5COR) and that with N termini inward (gray, PDB ID code 2X69). Chain F was used for alignment. Chain F and Chain G have outward N termini. The close-up view shows gained hydrogen bonds (right, top) or lost hydrogen bonds (right, bottom) for CCL3 with N termini pointing outward. (*D*) Electrostatic surface potential of CCL3 decamer with N termini pointing outward (*Top*) and that with all *N*-termini pointing inward (*Bottom*). The decamer surface is colored from negative (red −1 kT) to positive (blue +1 kT).

Our structural studies also offer additional mechanisms for regulating the coupling of oligomerization and GAG binding. We found an N-terminal flipped conformation of CCL3 within CCL3 oligomers, which likely occurs naturally due to the flexible nature of CCL3 N terminus. This conformation has a reduced dimer–dimer interface, which should destabilize it relative to the nonflipped conformation and thus depolymerize more readily. This conformation, however, has a larger positively charged pocket so it could have a higher affinity for GAGs than the nonflipped conformation (Fig. 5*D*). This is consistent with the fact that this crystal form is more readily formed when **8f** was present. Thus, the presence of GAG would promote the dissociation of CCL3 oligomers by weakening the interaction between CCL3 dimers. This offers a means by which conformational switches can regulate CCL3 oligomerization and explains how CCL3 forms shorter oligomers in the presence of heparin (14).

Our CCL5 oligomeric structure can, in part, explain how oligomerization affects CCL5 functions by affecting its proteolytic sensitivity (Fig. 6*A*) (43). Only monomeric CC chemokines bind and activate their respective cognate CCRs. However, they are highly susceptible to proteolysis, particularly at their N termini, which is critical for receptor binding and activation (44–46). In comparison, CC chemokine oligomers are resistant to proteases but receptor-binding-incompetent because oligomerization buries CCR-binding sites. Thus, dimerization and oligomerization prolong the half-life of CC chemokines while reducing the effectiveness of these chemokines. The N terminus of CCL5 can be cleaved by DPP IV and cathepsin G, thus altering the ability of CCL5 to activate its cognate receptors (43). Our CCL5 oligomeric structure reveals that the CCL5 N terminus is buried inside the concave surface of the oligomer, which should protect the oligomer from proteolytic inactivation. Oligomerization of CCL5 also buries substantial solvent-exposed areas. This should protect CCL5 from degradation by other extracellular proteases (e.g., tryptase) (43). We have proposed that the interplay between reversible oligomerization and protease sensitivity makes CCL3 and CCL4 more effective chemoattractants over a longer range and thus encodes severity during infection or inflammation (14) (Fig. 6*B*). This is applicable to CCL5 and other chemokine that can oligomerize (e.g., CCL2).

GAG binding in conjunction with oligomerization can profoundly affect the functions of CC chemokines. Similar to oligomerization, GAG binding could alter the chemotactic gradient of CC chemokines by modulating their sensitivity to proteases (Fig. 6*C*). GAG could bring multiple CC chemokine oligomers together (Fig. 6*C*). Consistent with this notion, analysis of symmetry-related molecules in our structure indicates that long-chain GAGs can bring two CCL3 oligomers together (Fig. S4 *B* and *C*). GAG-mediated aggregation of CC chemokine oligomers could further increase the local concentration of CC chemokines to regulate the activation of cognate CCRs and the presentation of CC chemokines to circulating lymphocytes (Fig. 6*C*). This would also promote the formation of high-MW CC chemokine oligomers in the extracellular matrix and on cell surfaces (Fig. 6*C*). The oligomerization of CC chemokines and novel GAG binding of CC chemokine oligomers could facilitate the aggregation of proteoglycan (e.g., CD44), which in turn promotes non-CCR mediated signaling (e.g., tyrosine phosphorylation) (Fig. 6*C*). Given the complexity of how chemokines recruit immune cells, which involves cell arrest and adhesion onto the endothelial cells, extravasation across blood vessels, and cell migration toward the source of the CC chemokines, future investigation will be required to elucidate how the GAG binding and oligomerization of CC chemokines are coupled to affect each step of chemokine-mediated cell recruitment under normal physiological and pathological settings.

Methods

Chemokine Expression and Purification, Crystallization, Data Collection, and Structure Determination. The expression of thioreduxin-tagged CCL5, CCL5(4-68), and CCL3 in *Escherichia coli*, the removal of thioreduxin-tag by enterokinase or tobacco etch virus (TEV) protease, and the purification of these chemokines by Ni-NTA, source-Q, and heparin columns are done similar to methods described previously (14, 47). The octasaccharide heparin MLZ-**8f** was synthesized as described (35). Crystals of CC chemokines in the presence and absence of heparin **8f** were grown using hanging-drop vapor diffusion

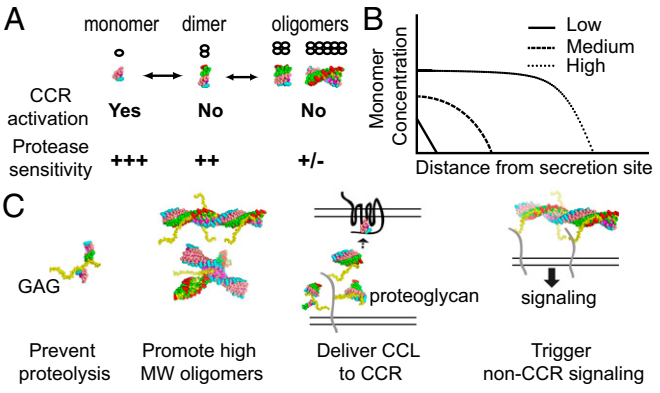

Fig. 6. Roles of oligomerization, GAG binding, and proteolytic degradation of CC chemokines. (*A*) Equilibrium of CC chemokine oligomeric states and their properties in receptor binding and protease sensitivity. (*B*) Distribution of monomeric CC chemokine (log scale) from the source over the distance (linear scale). At low and medium levels of CC chemokine where it is most monomer or a mixture of monomer and dimer, respectively, cells will be directed to the center of CC chemokine source. However, at high CC chemokine level where it also forms oligomer, cells will only be migrated to the peripheral of CC chemokine source, rather than to the center. This would help to prevent the spread of invading pathogens in a severe infection. This is because the difference in CC chemokine monomer level within the cell length is less than required difference for the effective chemotaxis. (*C*) Effects of GAG binding and oligomerization to the functions of CC chemokines (see *Discussion*).

and cryoprotected under the conditions listed in Table S2. Diffraction data were collected at 100 K at beamline 19-ID or 19-BM at Advanced Photon Source, Argonne National Laboratory and processed with HKL3000 (48). Molecular replacement was done using Phaser (49) and structural refinement and rebuilding were performed with Coot (50) and Phenix (51–53). Further details are provided in *SI Methods*.

SAXS Data Acquisition and Analysis. SAXS data were collected at the BioCAT/18ID beamline at Advanced Photon Source, Argonne National Laboratory. Chemokine [0.6 mg/mL CCL5, 0.9 mg/mL CCL5(4-68), and 1 mg/mL CCL3] in the presence or absence of 1–10 μg/mL heparin (Alfa Aesar) in the buffer containing 20 mM Tris·HCl (pH 8.0), 500 mM NaCl, 1 mM EDTA, and 1 mM β-mercaptoethanol was used for data collection. ATSAS package, Primus, and Crysol were used for data reduction and analysis (53, 54). A simple scheme for polymerization assuming equal probability of binding or unbinding between dimers independent of location was used to generate a model of oligomer size distribution to fit the SAXS data (14, 37). Further details are provided in *SI Methods*.

ACKNOWLEDGMENTS. We thank Andrew Wang, John King, Mara Farcasanu, Stephanie Tang, and Krishna Rajarathnam for helpful comments and the staff of APS SBC and BioCAT for assisting with data collection. This work was supported by NIH Grant GM81539, Institute of Translational Medicine Grant CTSA UL1 TR000430, University of Chicago BSD bridge funding (W.-J.T.), Mizutani Foundation for Glycoscience, Academia Sinica, the Ministry of Science and Technology of Taiwan Grants 104-0210-01-09-02 and 104-2628-M-001-001 (to S.-C.H.), Grant P41 GM103622 to BioCAT, NIH Grant T32EB009412, and National Science Foundation Grant DGE-1144082. Use of the Advanced Photon Source was supported by the US Department of Energy, Office of Basic Energy Sciences, under Contract W-31-109-ENG-38.

1. Allen SJ, Crown SE, Handel TM (2007) Chemokine: Receptor structure, interactions, and antagonism. *Annu Rev Immunol* 25:787–820.
2. Lazennec G, Richmond A (2010) Chemokines and chemokine receptors: New insights into cancer-related inflammation. *Trends Mol Med* 16(3):133–144.
3. Xu D, Esko JD (2014) Demystifying heparan sulfate-protein interactions. *Annu Rev Biochem* 83(1):129–157.
4. Handel TM, Johnson Z, Crown SE, Lau EK, Proudfoot AE (2005) Regulation of protein function by glycosaminoglycans–as exemplified by chemokines. *Annu Rev Biochem* 74:385–410.
5. Koenen RR, Weber C (2010) Therapeutic targeting of chemokine interactions in atherosclerosis. *Nat Rev Drug Discov* 9(2):141–153.
6. Varki A, et al. (2009) *Essentials of Glycobiology* (Cold Spring Harbor Lab Press, Cold Spring Harbor, NY), 2nd Ed.
7. Salanga CL, Handel TM (2011) Chemokine oligomerization and interactions with receptors and glycosaminoglycans: The role of structural dynamics in function. *Exp Cell Res* 317(5):590–601.
8. Fu L, Suflita M, Linhardt RJ (2016) Bioengineered heparins and heparan sulfates. *Adv Drug Deliv Rev* 97:237–249.
9. Jones KL, Maguire JJ, Davenport AP (2011) Chemokine receptor CCR5: From AIDS to atherosclerosis. *Br J Pharmacol* 162(7):1453–1469.
10. Kanzler I, Liehn EA, Koenen RR, Weber C (2012) Anti-inflammatory therapeutic approaches to reduce acute atherosclerotic complications. *Curr Pharm Biotechnol* 13(1):37–45.
11. Clemons MJ, et al. (1998) A randomized phase-II study of BB-10010 (macrophage inflammatory protein- 1α) in patients with advanced breast cancer receiving 5-fluorouracil, adriamycin, and cyclophosphamide chemotherapy. *Blood* 92(5):1532–1540.
12. Kanegasaki S, Matsushima K, Shiraishi K, Nakagawa K, Tsuchiya T (2014) Macrophage inflammatory protein derivative ECI301 enhances the alarmin-associated abscopal benefits of tumor radiotherapy. *Cancer Res* 74(18):5070–5078.
13. Graham GJ, et al. (1994) Aggregation of the chemokine MIP-1 α is a dynamic and reversible phenomenon. Biochemical and biological analyses. *J Biol Chem* 269(7):4974–4978.
14. Ren M, et al. (2010) Polymerization of MIP-1 chemokine (CCL3 and CCL4) and clearance of MIP-1 by insulin-degrading enzyme. *EMBO J* 29(23):3952–3966.
15. Czaplewski LG, et al. (1999) Identification of amino acid residues critical for aggregation of human CC chemokines macrophage inflammatory protein (MIP)-1α, MIP-1β, and RANTES. Characterization of active disaggregated chemokine variants. *J Biol Chem* 274(23):16077–16084.
16. Appay V, Brown A, Cribbes S, Randle E, Czaplewski LG (1999) Aggregation of RANTES is responsible for its inflammatory properties. Characterization of nonaggregating, noninflammatory RANTES mutants. *J Biol Chem* 274(39):27505–27512.
17. Baltus T, Weber KSC, Johnson Z, Proudfoot AEI, Weber C (2003) Oligomerization of RANTES is required for CCR1-mediated arrest but not CCR5-mediated transmigration of leukocytes on inflamed endothelium. *Blood* 102(6):1985–1988.
18. Proudfoot AEI, et al. (2003) Glycosaminoglycan binding and oligomerization are essential for the in vivo activity of certain chemokines. *Proc Natl Acad Sci USA* 100(4):1885–1890.
19. Appay V, et al. (2000) RANTES activates antigen-specific cytotoxic T lymphocytes in a mitogen-like manner through cell surface aggregation. *Int Immunol* 12(8):1173–1182.
20. Murooka TT, et al. (2006) CCL5-CCR5-mediated apoptosis in T cells: Requirement for glycosaminoglycan binding and CCL5 aggregation. *J Biol Chem* 281(35):25184–25194.
21. Roscic-Mrkic B, et al. (2003) RANTES (CCL5) uses the proteoglycan CD44 as an auxiliary receptor to mediate cellular activation signals and HIV-1 enhancement. *Blood* 102(4):1169–1177.
22. Iida N, et al. (2010) Antitumor effect after radiofrequency ablation of murine hepatoma is augmented by an active variant of CC Chemokine ligand 3/macrophage inflammatory protein-1α. *Cancer Res* 70(16):6556–6565.
23. Wagner L, et al. (1998) β-chemokines are released from HIV-1-specific cytolytic T-cell granules complexed to proteoglycans. *Nature* 391(6670):908–911.
24. Øynebråten I, et al. (2015) Oligomerized, filamentous surface presentation of RANTES/CCL5 on vascular endothelial cells. *Sci Rep* 5:9261.
25. Chung CW, Cooke RM, Proudfoot AE, Wells TN (1995) The three-dimensional solution structure of RANTES. *Biochemistry* 34(29):9307–9314.
26. Hoover DM, et al. (2000) The crystal structure of Met-RANTES: Comparison with native RANTES and AOP-RANTES. *Protein Pept Lett* 7(2):73–82.
27. Jin H, Kagiampakis I, Li P, Liwang PJ (2010) Structural and functional studies of the potent anti-HIV chemokine variant P2-RANTES. *Proteins* 78(2):295–308.
28. Shaw JP, et al. (2004) The X-ray structure of RANTES: Heparin-derived disaccharides allows the rational design of chemokine inhibitors. *Structure* 12(11):2081–2093.
29. Wang X, Watson C, Sharp JS, Handel TM, Prestegard JH (2011) Oligomeric structure of the chemokine CCL5/RANTES from NMR, MS, and SAXS data. *Structure* 19(8):1138–1148.
30. Wilken J, et al. (1999) Total chemical synthesis and high-resolution crystal structure of the potent anti-HIV protein AOP-RANTES. *Chem Biol* 6(1):43–51.
31. Brandner B, Rek A, Diedrichs-Möhring M, Wildner G, Kungl AJ (2009) Engineering the glycosaminoglycan-binding affinity, kinetics and oligomerization behavior of RANTES: A tool for generating chemokine-based glycosaminoglycan antagonists. *Protein Eng Des Sel* 22(6):367–373.
32. Raman R, Sasisekharan V, Sasisekharan R (2005) Structural insights into biological roles of protein-glycosaminoglycan interactions. *Chem Biol* 12(3):267–277.
33. Zulueta MML, Lin S-Y, Hu Y-P, Hung S-C (2013) Synthetic heparin and heparan sulfate oligosaccharides and their protein interactions. *Curr Opin Chem Biol* 17(6):1023–1029.
34. Lortat-Jacob H, Grosdidier A, Imberty A (2002) Structural diversity of heparan sulfate binding domains in chemokines. *Proc Natl Acad Sci USA* 99(3):1229–1234.
35. Zulueta MML, et al. (2012) α-Glycosylation by D-glucosamine-derived donors: Synthesis of heparosan and heparin analogues that interact with mycobacterial heparin-binding hemagglutinin. *J Am Chem Soc* 134(21):8988–8995.
36. Hu Y-P, et al. (2012) Divergent synthesis of 48 heparan sulfate-based disaccharides and probing the specific sugar-fibroblast growth factor-1 interaction. *J Am Chem Soc* 134(51):20722–20727.
37. Vandongen PGJ, Ernst MH (1984) Kinetics of reversible polymerization. *J Stat Phys* 37(3–4):301–324.
38. Segerer S, et al. (2009) The basic residue cluster (55)KKWVR(59) in CCL5 is required for in vivo biologic function. *Mol Immunol* 46(13):2533–2538.
39. Proudfoot AE, et al. (2001) The BBXB motif of RANTES is the principal site for heparin binding and controls receptor selectivity. *J Biol Chem* 276(14):10620–10626.
40. Koenen RR, et al. (2009) Disrupting functional interactions between platelet chemokines inhibits atherosclerosis in hyperlipidemic mice. *Nat Med* 15(1):97–103.
41. von Hundelshausen P, et al. (2005) Heterophilic interactions of platelet factor 4 and RANTES promote monocyte arrest on endothelium. *Blood* 105(3):924–930.
42. Dyer DP, Salanga CL, Volkman BF, Kawamura T, Handel TM (2016) The dependence of chemokine-glycosaminoglycan interactions on chemokine oligomerization. *Glycobiology* 26(3):312–326.
43. Mortier A, Gouwy M, Van Damme J, Proost P (2011) Effect of posttranslational processing on the in vitro and in vivo activity of chemokines. *Exp Cell Res* 317(5):642–654.
44. Paavola CD, et al. (1998) Monomeric monocyte chemoattractant protein-1 (MCP-1) binds and activates the MCP-1 receptor CCR2B. *J Biol Chem* 273(50):33157–33165.
45. Qin L, et al. (2015) Structural biology. Crystal structure of the chemokine receptor CXCR4 in complex with a viral chemokine. *Science* 347(6226):1117–1122.
46. Kufareva I, Salanga CL, Handel TM (2015) Chemokine and chemokine receptor structure and interactions: Implications for therapeutic strategies. *Immunol Cell Biol* 93(4):372–383.
47. Liang WG, Ren M, Zhao F, Tang W-J (2015) Structures of human CCL18, CCL3, and CCL4 reveal molecular determinants for quaternary structures and sensitivity to insulin-degrading enzyme. *J Mol Biol* 427(6 Pt B):1345–1358.
48. Minor W, Cymborowski M, Otwinowski Z, Chruszcz M (2006) HKL-3000: The integration of data reduction and structure solution–from diffraction images to an initial model in minutes. *Acta Crystallogr D Biol Crystallogr* 62(Pt 8):859–866.
49. McCoy AJ, et al. (2007) Phaser crystallographic software. *J Appl Cryst* 40(Pt 4):658–674.
50. Emsley P, Cowtan K (2004) Coot: Model-building tools for molecular graphics. *Acta Crystallogr D Biol Crystallogr* 60(Pt 12 Pt 1):2126–2132.
51. Afonine PV, et al. (2012) Towards automated crystallographic structure refinement with phenix.refine. *Acta Crystallogr D Biol Crystallogr* 68(Pt 4):352–367.
52. Terwilliger TC, et al. (2009) Decision-making in structure solution using Bayesian estimates of map quality: The PHENIX AutoSol wizard. *Acta Crystallogr D Biol Crystallogr* 65(Pt 6):582–601.
53. Konarev PV, Volkov VV, Sokolova AV, Koch MH, Svergun DI (2003) PRIMUS: A Windows PC-based system for small-angle scattering data analysis. *J Appl Cryst* 36(5):1277–1282.
54. Petoukhov MV, et al. (2012) New developments in the ATSAS program package for small-angle scattering data analysis. *J Appl Cryst* 45(Pt 2):342–350.
55. Svergun D, Barberato C, Koch M (1995) CRYSOL – A program to evaluate X-ray solution scattering of biological macromolecules from atomic coordinates. *J Appl Cryst* 28(6):768–773.